

Two Binding Orientations for Peptides to the Src SH3 Domain: Development of a General Model for SH3-Ligand Interactions

Sibo Feng, James K. Chen, Hongtao Yu, Julian A. Simon, Stuart L. Schreiber*

Solution structures of two Src homology 3 (SH3) domain–ligand complexes have been determined by nuclear magnetic resonance. Each complex consists of the SH3 domain and a nine-residue proline-rich peptide selected from a large library of ligands prepared by combinatorial synthesis. The bound ligands adopt a left-handed polyproline type II (PPII) helix, although the amino to carboxyl directionalities of their helices are opposite. The peptide orientation is determined by a salt bridge formed by the terminal arginine residues of the ligands and the conserved aspartate-99 of the SH3 domain. Residues at positions 3, 4, 6, and 7 of both peptides also intercalate into the ligand-binding site; however, the respective proline and nonproline residues show exchanged binding positions in the two complexes. These structural results led to a model for the interactions of SH3 domains with proline-rich peptides that can be used to predict critical residues in complexes of unknown structure. The model was used to identify correctly both the binding orientation and the contact and noncontact residues of a peptide derived from the nucleotide exchange factor Sos in association with the amino-terminal SH3 domain of the adaptor protein Grb2.

The Src tyrosine kinase has an NH₂-terminal SH3 domain that negatively regulates its kinase activity (1). SH3 domains are present in several intracellular proteins and mediate protein-protein interactions important in cytoskeletal architecture and intracellular signaling (2). The identification of several SH3-binding proteins by expression cloning and affinity chromatography demonstrated that SH3 domains bind to proline-rich sequences (3). SH3 domains also have specific preferences for arginine and leucine residues, as revealed by the use of combinatorial peptide libraries with the Src and phosphatidylinositol 3-kinase (PI3K) SH3 domains (4, 5). These studies identified two classes of ligands for both SH3 domains: class I, with the consensus sequence RXLPPZP (Z = L for Src SH3; Z = R for PI3K SH3; X means no clear consensus was found), and class II, with the sequence XPPLPXR (6).

Recent structures of SH3 domains from PI3K, Abl, and Fyn complexed with proline-rich ligands indicate that the ligands adopt a PPII helix conformation (5, 7). The complexes are stabilized predominantly by hydrophobic contacts and, in the case of PI3K SH3, by additional electrostatic interactions between the arginine residues of the peptide RLP1 (the class I ligand RKLP-PRPSK) and D21 and E51 of the protein. In all three complexes, the ligands adopt a similar binding mode, with the peptide backbones oriented in the same direction.

Because class I peptides contain a conserved NH₂-terminal arginine that is critical for SH3 binding, whereas class II peptides contain a conserved COOH-terminal arginine, it was suggested that peptides of the two classes might bind to SH3 domains in reverse orientations (4, 5). To address this possibility of dual binding modes, we have now determined the solution structures of c-Src SH3 complexed with a class I peptide RALPPLPRY (RLP2) and a class II peptide AFAPPLPRR (PLR1) by multidimensional nuclear magnetic resonance (NMR) spectroscopy (8–11). Although both peptides adopt a PPII helix conformation, they bind to the SH3 domain in reverse orientations.

The superimposed α -carbon traces of the 20 final structures for the two complexes are shown in Fig. 1 and a summary of the energetic and geometric statistics of the two sets of structures is provided in Table 1. The ligand-bound conformations of the Src SH3 domain in both complexes are essentially identical to that of the unbound state. The SH3 domain consists of two three-stranded antiparallel β sheets, with two loops from residues 93 to 99 and from 112 to 117 (12). The backbone root-mean-square deviation between the minimized average structures of the RLP2-bound and -unbound forms of the SH3 domain is 1.14 Å; the corresponding value for the PLR1-bound and -unbound forms is 1.17 Å. There is, however, one important difference between the bound and unbound states of the Src SH3 domain revealed by hydrogen-deuterium exchange experiments (10). Eleven slowly exchanging amide protons exist in RLP2-bound SH3 (10 for PLR1-bound SH3),

compared with only three in the unbound state. These additional slowly exchanging amide protons are located on the two β sheets, at positions both near and distant to the ligand-binding site. Ligand complexation thus appears to retard the cooperative unfolding of the SH3 domain (13). Both ligands adopt an extended conformation, with residues 1 to 7 of RLP2 and residues 3 to 9 of PLR1 forming left-handed PPII helices in which all prolines are in a trans configuration.

In the RLP2-SH3 structure, the class I peptide RLP2 binds with the same orientation as the ligands in previously determined SH3-ligand complexes (Figs. 1A and 2, A and B) (5, 7). Because the PPII helix conformation has three residues per turn, residues at positions *i* and *i* + 3 lie on the same edge of the helix. Residues R1, P4, and P7 form one edge of the PPII helix that interacts with the protein and L3 and L6 form another protein-contacting edge. The ligand-binding site on the SH3 domain contains three binding pockets. The first is an arginine-binding pocket that accommodates the NH₂-terminal R1 of RLP2 and is positioned between W118 and D99 of the protein (position P_I) (Fig. 3A). The side chain of R1 packs against the indole ring of W118 (Fig. 2, A and B). The relative positions of the R1 carbonyl oxygen and the indole N–H of W118 allow for a possible hydrogen bond between them, in analogy to the hydrogen bond in the Abl SH3–ligand complex (7, 14). The guanidinium group of R1 is proximal to the acidic side chain of D99. This residue is structurally equivalent to D21 in the RLP1–PI3K SH3 complex, which was found to form a salt bridge with R1 of RLP1 (5). A similar salt bridge appears to exist between R1 of RLP2 and D99 of Src SH3 because the amide proton chemical shift of D99 is significantly perturbed on RLP2 binding, and the D99N mutant of Src SH3 binds to RLP2 with a ~40-fold decrease in affinity (Table 2) (15, 16). The second (positions P_{II} and P_V) and third (positions P_{III} and P_{IV}) (Fig. 3A) pockets each accommodate a proline residue. Residues Y92, W118, P133, and Y136 form the second pocket and make extensive hydrophobic contacts with L3 and P4 of RLP2. The methyl groups of L3 also contact the side chains of D117 and N135 in the protein. L6 and P7 of RLP2 interact with the third binding pocket formed by Y90 and Y136. The disordered COOH-terminal residues R8 and Y9 of RLP2 do not contact the SH3 domain (17).

The overall similarity between the structures of RLP1–PI3K SH3 and RLP2–Src SH3 suggests that all class I ligands adopt the same binding mode. There are, however, differences in the two structures that exemplify the specificity of SH3-ligand rec-

Howard Hughes Medical Institute, Department of Chemistry, Harvard University, Cambridge, MA 02138, USA.

*To whom correspondence should be addressed.

ognition. The class I ligands for PI3K SH3 have a conserved arginine at position 6, whereas those for Src SH3 contain leucine. This selection has been attributed to the 15-residue acidic insert specific to PI3K SH3. Residue E51 of this insert forms a salt bridge with R6 of RLP1, resulting in a small change in the relative positions of the peptide backbones of RLP1 and RLP2. The side chain of L6 in RLP2 is structurally better defined than that of R6 in RLP1 because of the extensive hydrophobic contacts between L6 and the receptor. Relative residue positions within the proline-binding pocket also differ slightly between the two structures; for example, P4 of RLP2 binds more deeply into its binding pocket than P4 of RLP1.

The structure of the class II ligand PLR1 complexed to the SH3 domain of Src reveals a binding mode not observed previously. Although PLR1 interacts with the

receptor through the same three binding pockets as does RLP2, its amide backbone directionality is reversed relative to that of RLP2 (Figs. 1 and 2). The COOH-terminal R9 of PLR1 occupies the arginine-binding pocket (P_{II}), where its side chain packs against the W118 indole ring (Figs. 2 and 3B). Analogous to the NH_2 -terminal arginines of RLP1 and RLP2, R9 forms a salt bridge to D99 of Src SH3 (15). The presence of this salt bridge is also consistent with mutational studies: Replacing R9 with an alanine results in a similar ≥ 10 -fold decrease in affinity as seen when D99 is mutated to an asparagine (Table 2). Furthermore, the amide proton chemical shift of D99 is significantly perturbed on PLR1 complexation with a pattern similar to that observed with RLP2. As a result of the reverse backbone directionality relative to the RLP-type ligands, L6 and P7 of PLR1 intercalate into the second binding pocket,

whereas A3 and P4 bind to the third pocket (Fig. 2, A and C). The opposite orientations of the two P_{II} helices also result in an exchange of positions of the prolines and nonproline residues. Specifically, P4 and P7 of PLR1 assume the respective positions of L6 and L3 in RLP2, whereas A3 and L6 of PLR1 occupy those of P7 and P4 in RLP2, respectively. The positional interchange explains the selection of leucine at position 6 in the class II ligand sequences for both PI3K and Src SH3 domains, because this residue is located in a hydrophobic pocket that is distant from the PI3K SH3 acidic insert. Other PLR1 residues do not contact the protein; the side chains of P5 and R8 are oriented toward the solvent. The NH_2 -terminal residues A1 and F2 of PLR1 are structurally disordered.

The overall hydrophobic contact between the peptide and its receptor is less for PLR1 than for RLP2 because of the short side chain of A3 in PLR1. Furthermore, the proline rings of P4 and P7 of PLR1 cannot undergo the same extensive hydrophobic interactions with the side chains of D117 and N135 as do the extended side chains of L3 and L6 in RLP2. Thus, the variation in affinity between the two ligands and Src SH3 (Table 2) appears attributable to differences in hydrophobic contacts. The lower affinity of PLR1 for Src SH3 may not represent a general phenomenon for class II ligands, however, because the class II peptide LNKPPPKR binds to PI3K SH3 with a dissociation constant (K_d) of 13 μM (5).

Individual residues of the PLR1 peptide were replaced by alanine or glycine to determine their relative importance for SH3 binding (Table 2). The results of these studies are consistent with the structure in that the contact residues (A3, P4, L6, P7, and R9) contribute most to the binding, whereas mutations of the two disordered NH_2 -terminal residues (A1 and F2) and the non-contacting residue R8 have little effect on binding affinity. The scaffolding proline P5, though not contacting the protein, can stabilize the formation of the P_{II} helix, and its mutation to alanine results in an anticipated small decrease in binding affinity.

For both RLP2 and PLR1 peptides, a conserved XPpXP motif (P, SH3-contacting proline; p, scaffolding proline) containing P4 and P7 is essential for SH3 binding (18). The second and third binding pockets of the SH3 domain can accommodate the XP dipeptidyl moieties in two orientations. These two XP moieties are linked by a scaffolding proline to stabilize the P_{II} helix (Figs. 2 and 3). In the complexes, P4 and P7 of RLP2 are located at positions P_{II} and P_{III} , whereas those of PLR1 are located at positions P_{IV} and P_V (Fig. 3). In the structure of Abl SH3 complexed with a 3BP1-derived peptide, APTMPPLPP, that

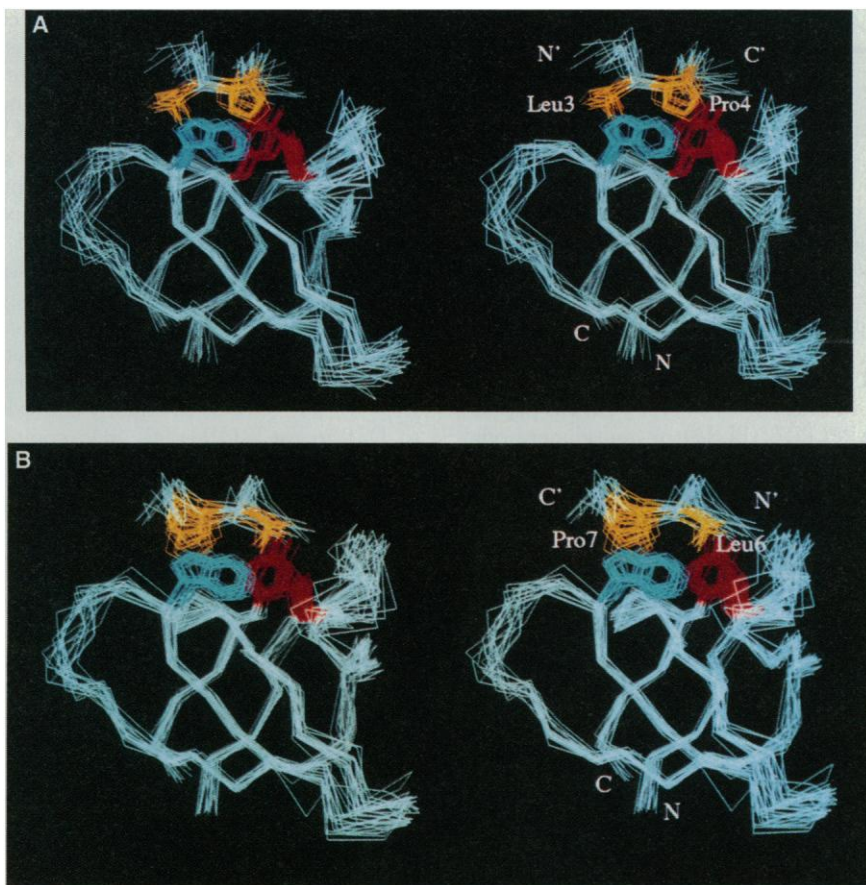


Fig. 1. Stereoviews of the superposition of 20 final refined structures of the RLP2-Src SH3 complex (A) and the PLR1-Src SH3 complex (B). The α -carbon traces are light blue, L3 and P4 of RLP2 and L6 and P7 of PLR1 are yellow. Three residues at the binding site are also shown, with W118 in blue and Y92 and Y136 (in the back) in red. The NH_2 - and COOH-termini of Src SH3 are labeled N and C, respectively, and those of the ligands are labeled N' and C' , respectively. Excluding the less well defined loop regions of the SH3 domain (residues 94 to 98 and residues 113 to 116) and the disordered residues of the ligands (residues 8 and 9 of RLP2 and residues 1 and 2 of PLR1), the average root-mean-square deviations of the 20 structures against their mean coordinate are 0.69 \AA for the backbone atoms and 1.07 \AA for all heavy atoms for the RLP2-SH3 complex; the corresponding deviations for the PLR1-SH3 complex are 0.72 and 1.23 \AA , respectively. None of the structures shows nuclear Overhauser effect violations of $>0.3 \text{\AA}$ or dihedral angle violations of $>3^\circ$. The atomic coordinates of the 20 final structures for both complexes have been deposited in the Brookhaven Protein Data Bank.

Table 1. Structural and energetic statistics for the complexes of RLP2–Src SH3 and PLR1–Src SH3. The SA_i columns give the mean ± SD values for the indicated variables obtained from the 20 final refined simulated annealing (SA)

structures. (SA)_{ref} represents minimized mean structure obtained from individual SA structures best fitted to each other. The numbers of various restraints are given in parentheses.

Parameter	RLP2–Src SH3		PLR1–Src SH3	
	SA _i	(SA) _{ref}	SA _i	(SA) _{ref}
<i>Root-mean-square deviations from experimental distance restraints (Å)</i>				
All	(715)	0.013 ± 0.002	0.016	(668)
Interproton distances of Src SH3				
Intraresidue	(207)	0.014 ± 0.004	0.018	(206)
Interresidue sequential ($ i - j = 1$)	(173)	0.015 ± 0.005	0.017	(173)
Interresidue short range ($1 < i - j \leq 5$)	(29)	0.009 ± 0.006	0.017	(29)
Interresidue long range ($ i - j > 5$)	(171)	0.008 ± 0.003	0.011	(171)
Hydrogen bond restraints*	(26)	0.010 ± 0.003	0.011	(24)
Interproton distances of RLP2	(62)	0.018 ± 0.001	0.017	
Interproton distances of PLR1				(31)
Intermolecular ligand-SH3 interproton distances	(47)	0.004 ± 0.002	0.013	(34)
<i>Root-mean-square dihedral deviations (degrees)</i>				
All	(52)	0.121 ± 0.068	0.151	(52)
<i>Deviations from idealized geometry†</i>				
Bonds (Å)	(1053)	0.005 ± 0.000	0.005	(1043)
Angles (degrees)	(1889)	1.613 ± 0.003	1.619	(1870)
Impropers (degrees)	(496)	0.154 ± 0.018	0.158	(496)
<i>Energetic statistics (kcal mol⁻¹)</i>				
E_{repel}^\ddagger		5.0 ± 2.0	7.8	
E_{vdw}^\S		-111.1 ± 24.1	-138.6	
E_{NOE}^\P		6.2 ± 2.1	8.7	
				5.4 ± 3.8
				-123.7 ± 14.4
				9.5
				-159.8
				7.4

*Four of the distance restraints were derived from the two hydrogen bonds that are conserved in all the calculated structures and located at the center of the β sheet; all other hydrogen bond restraints were from slowly exchanging amide protons. †Idealized geometries based on CHARMM 19 parameters (30). ‡Repulsive potential. The value of the quartic repulsive force constant used in the structure calculations was 4 kcal mol⁻¹ Å⁻⁴. §Lennard-Jones van der Waals energy calculated with standard CHARMM 19 parameters (30). ¶Total distance restraint energy. The values of the square-well NOE and torsion angle force constants were 50 kcal mol⁻¹ Å⁻² and 200 kcal mol⁻¹ rad⁻², respectively.

adopts the RLP-type orientation, the prolines at positions 6, 7, 9, and 10 of the peptide (in boldface) occupy binding positions P_V, P_{II}, P_{IV}, and P_{III}, respectively (7). Mutating P6 or P9 to alanine does not affect SH3 binding significantly. In contrast, replacing P7 or P10 with alanine abolishes binding (19). Accordingly, SH3 ligands that adopt an RLP-type orientation (class I) on binding prefer to have their two critical prolines of the XPpXP motif contacting the P_{II} and P_{III} sites, whereas PLR-type (class II) ligands prefer to have these

prolines contacting the P_{IV} and P_V sites.

In considering possible reasons why XP dipeptidyl moieties are selected by SH3 domains over PX ones (X, nonproline residue), the van der Waals surface of an XP sequence in a PPII helix is structurally more compact than that of PX. This appears to

allow a better fit of the XP moieties into the hydrophobic clefts (Fig. 2). The side chain substituent of residue X is only two bonds away from the proline ring in XP (the two bonds are C_α-CO and CO-N) (Fig. 4A). In contrast, for a PX sequence, the side chain of X is three bonds away from the proline

Table 2. Mutational analysis of RLP2 and PLR1.

Src SH3 domain	Peptide*	K _d (μM)†
Wild-type	RALPPLPRY	8.0 ± 0.3
D99N	RALPPLPRY	310 ± 70
Wild-type	AFAPPLPRR	59 ± 4
	GF APPLPRR	51 ± 5
	AA APPLPRR	65 ± 4
	AFG PPLPRR	69 ± 6
	AFAA PLPRR	>500
	AFAP AL PRR	75 ± 6
	AFAP PA PRR	>500
	AFAPPL AR	>500
	AFAPPL PA R	50 ± 4
	AFAPPL PR A	>500
D99N	AFAPPLPRR	>500

*All peptides were synthesized with free NH₂-termini and carboxamide COOH-termini. Boldface indicates mutated residues. †K_d values were measured by fluorescence spectroscopy (4) and are means ± SD of two independent determinations.

Table 3. Sequence alignment of SH3-binding motifs.

SH3-binding motif	Sequence									
Class I consensus*	X ₁	p	X ₂	P	p	X ₃	P			
Synthetic library consensus for Src	R	X	L	P	P	L	P			
Synthetic library consensus for PI3K	R	X	L	P	P	R	P			
Phage library consensus for Fyn	R	P	L	P	P	I/L	P			
Phage library consensus for Lyn	R	P	L	P	P	L	P			
Chicken YAP65 (239–247)	V	K	Q	P	P	L	A	P		
Human Btk (184–192)	T	K	K	P	L	P	T	P		
Human Btk (198–206)	L	K	K	P	L	P	E	P		
Human CDC42 GAP (250–258)	A	P	K	P	M	P	R	P		
Human C3G (604–612)	E	L	A	P	P	A	L	P		
Human dynamin (781–789)	P	Q	R	R	A	A	V	P		
Human p22 ^{phox} (151–159)	P	P	S	N	P	P	R	P		
Human PI3K p85 (91–99)	P	P	R	P	L	V	A	P		
Human PI3K p85 (303–311)	P	A	P	A	L	P	K	P		
Murine 3BP-1 (267–275)	P	T	M	P	P	L	P	P		
Murine 3BP-2-40 (2–10)	P	A	Y	P	P	P	V	P		
Class II consensus*	X ₃	P	p	X ₂	P	p	X ₁			
Synthetic library consensus for Src	X	P	P	L	P	X	R			
Synthetic library consensus for PI3K	X	P	P	L	P	X	R			
Human dynamin (812–820)	A	P	P	V	P	S	R	P	G	
Human p47 ^{phox} (362–370)	Q	P	A	V	P	P	R	P	S	
Murine Sos1 (1153–1161)	P	P	P	V	P	P	R	R	R	
Murine Sos1 (1214–1222)	P	P	L	L	P	P	R	E	P	
Murine Sos1 (1292–1300)	G	P	P	V	P	P	R	Q	S	

*The consensus sequences are defined in the text. Critical prolines of the XPpXP motif are in boldface.

ring (Fig. 4B), which results in a larger PX van der Waals surface that is not complementary to the hydrophobic clefts. XP is also conformationally more rigid than PX, because proline restricts the conformation of its preceding residue as a result of its special steric restraints (20).

Consistent with the model that XP is favored over PX, replacing the XP sequences of RLP2 and PLR1 with PX sequences resulted in a significant decrease in SH3 binding affinities. The PX peptides RPPLPPAP and PPLPPLPR (the PX sequences are in boldface) showed K_d values of 290 and 190 μ M with wild-type Src SH3, respectively, versus 8.0 and 59 μ M for the XP variants (Table 2). The first peptide was designed to bind to the SH3 domain in an RLP-type orientation, but with R1, P3, and P6 at the respective positions P_I , P_V , and P_{IV} . The second peptide was constructed to have a PLR-type binding orientation with P2, P5, and R8 at the respective positions P_{III} , P_{II} , and P_I (21). Other ligands such as the 3BP-1-derived peptide APTMPPPLPP exemplify the special instance in which the dipeptidyl moieties have PP sequences—prolines occupy positions P_{II} through P_V . As in RLP2 and PLR1, these protein-contacting PP moieties are structurally compact—the two pro-

line rings are two bonds apart—and are conformationally rigid. The combinatorial library studies with the Src and PI3K SH3 domains demonstrate, however, that the second and third binding pockets of these SH3 domains have a preference for XP sequences where X is not proline. This propensity for nonproline residues may reflect the ability of XP sequences (where X has an extended hydrophobic side chain, such as Leu and Val) to form composite binding surfaces that maximize hydrophobic interactions in the SH3-ligand complex.

The highly conserved binding sites in different SH3 domains and their preference for proline-rich ligands indicate that SH3-ligand interactions in the core binding region are governed by a common model. On the basis of the two binding modes revealed for the Src SH3-ligand complexes and other SH3-ligand structures, we describe the model as follows: (i) The binding site comprises conserved residues corresponding to Y90, Y92, D99, W118, Y131, P133, and Y136 of c-Src SH3. (ii) SH3 domains recognize proline-rich peptides that adopt a PPII helix conformation and two distinct binding modes exist that differ in the directionality of the ligand amide backbone. In either binding mode, a critical XPpXP motif

results in the intercalation of the two XP moieties into distinct hydrophobic pockets defined by conserved aromatic residues. The predominant driving force of the complexation is hydrophobic in nature, although it can be assisted by specific electrostatic and hydrogen bond interactions. (iii) For the RLP-type binding orientation (class I), the ligand consensus sequence is X_1 -p- X_2 -P-p- X_3 -P. For the PLR-type orientation (class II), the consensus is X_3 '-P-p- X_2 '-P-p- X_1 '. A lowercase p indicates a scaffolding residue that tends to be proline, whereas an uppercase P represents a critical SH3-contacting proline. X_i and X_i' represent important residues that also contact the receptor and can confer ligand specificity. X_1 and X_1' are preferentially arginines for SH3 domains possessing an acidic residue corresponding to D99 of Src SH3 (22). Most significantly, the salt bridge between the arginine and the acidic residue determines the ligand orientation. In the Abl SH3-binding proteins 3BP-1 and 3BP-2, X_1 is methionine or tyrosine (19), and the Abl SH3 has a compensating threonine instead of an acidic residue at the position corresponding to D99 of Src SH3. X_2 , X_2' , X_3 , and X_3' are usually hydrophobic residues, although, in PI3K SH3-binding se-

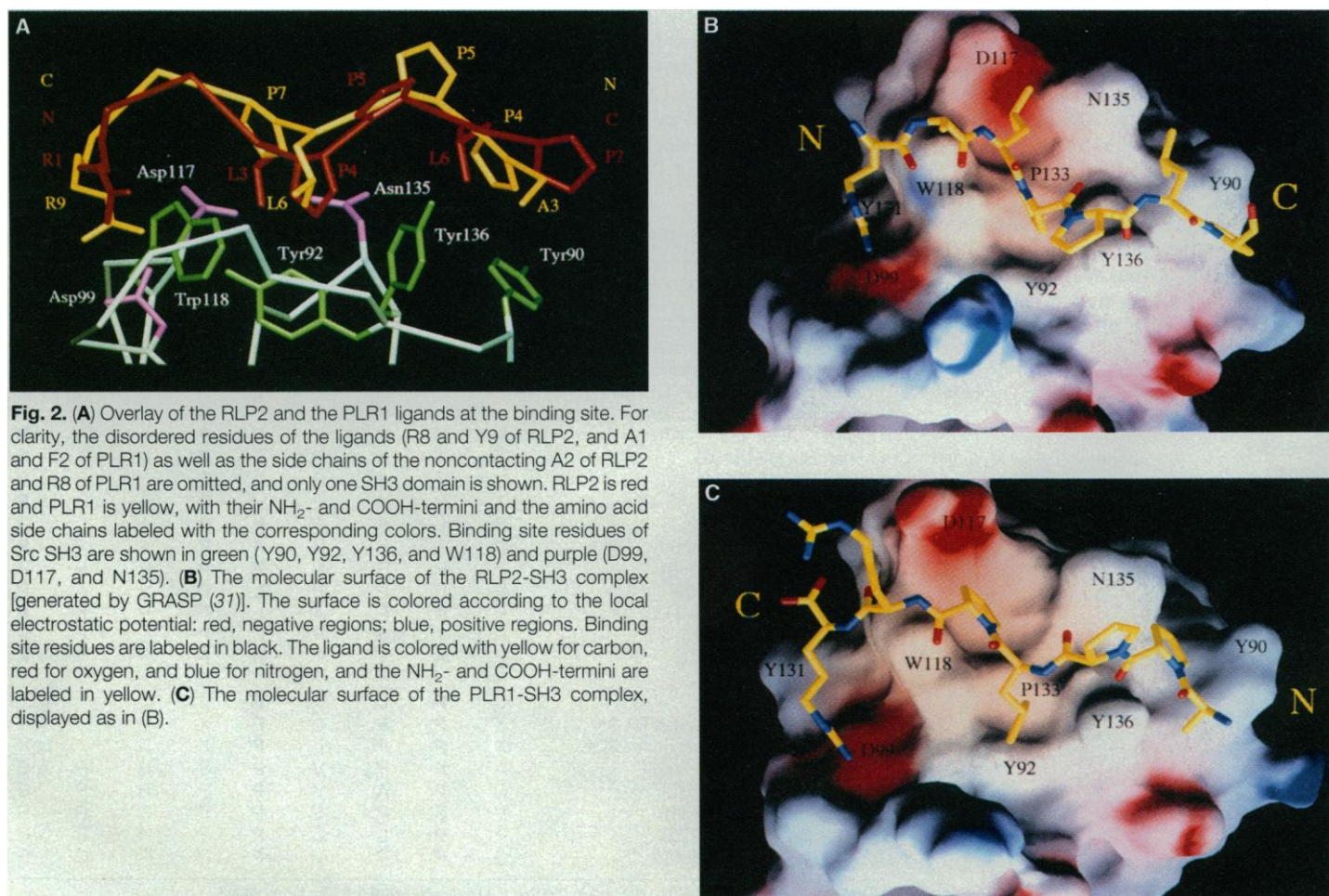


Fig. 2. (A) Overlay of the RLP2 and the PLR1 ligands at the binding site. For clarity, the disordered residues of the ligands (R8 and Y9 of RLP2, and A1 and F2 of PLR1) as well as the side chains of the noncontacting A2 of RLP2 and R8 of PLR1 are omitted, and only one SH3 domain is shown. RLP2 is red and PLR1 is yellow, with their NH_2 - and $COOH$ -termini and the amino acid side chains labeled with the corresponding colors. Binding site residues of Src SH3 are shown in green (Y90, Y92, Y136, and W118) and purple (D99, D117, and N135). (B) The molecular surface of the RLP2-SH3 complex [generated by GRASP (31)]. The surface is colored according to the local electrostatic potential: red, negative regions; blue, positive regions. Binding site residues are labeled in black. The ligand is colored with yellow for carbon, red for oxygen, and blue for nitrogen, and the NH_2 - and $COOH$ -termini are labeled in yellow. (C) The molecular surface of the PLR1-SH3 complex, displayed as in (B).

quences, X₃ is arginine, whose guanidinium group interacts with the extra acidic insert in PI3K SH3. The corresponding insert is basic in the neuronal Src SH3 domain, which therefore may select an acidic X₃. Prolines are preferred at the p positions to stabilize the formation of the PPII helix. Residues at these sites in natural sequences also tend to be hydrophobic as their side chains are expected to orient toward the interior of the SH3-binding proteins.

Both consensus sequences comprise seven residues and represent the core binding region of SH3 ligands. These residues occupy

three binding pockets in the SH3 domains, and their three-dimensional arrangement can be readily constructed with the mnemonic device shown in Fig. 3. Flanking residues outside this core—NH₂-terminal to X₁ and COOH-terminal to X₁—provide extra SH3-contacting elements that would be accommodated by one or more additional binding pockets. For example, the structure of Abl SH3 complexed with the peptide APTMPPPLPP reveals a fourth pocket located between W120 and W131 of Abl SH3 that interacts with the first two residues of the peptide [the two tryptophans correspond

to W118 and Y131 of Src SH3 (Fig. 2, B and C)]. Such flanking residues can contribute to SH3 binding (see below) (19, 23), although the mode of interaction is not well understood. In natural SH3-binding sequences, these flanking residues do not reveal a clear consensus, suggesting that they may be important in determining ligand specificity.

Naturally occurring peptide segments that have been shown to associate with SH3 domains possess either class I-like or class II-like sequences (Table 3) (3–5, 23–26). Proline, arginine, glutamine, serine, and alanine are the most preferred residues in PPII helices found in protein structures (27). In addition, the extended side chain methyl groups of leucine and valine can intercalate into the ligand-binding site of an SH3 domain efficiently. These same amino acids are the predominant ones found in natural SH3-binding sequences (Table 3). An example from these sequences that is highly homologous to the class I consensus is located COOH-terminal to the SH3 domain of the PI3K p85 subunit; it has the sequence RPLPVAP (residues 93 to 99). This region in p85 mediates the activation of the PI3K p110 subunit by binding to the Lyn or Fyn SH3 domains; it also mediates the dimerization of a recombinant p85 fragment by binding to the SH3 domain intermolecularly (26).

The physiological relevance of a class II-like sequence is exemplified by the association of the SH3 domains of Grb2 and the COOH-terminal proline-rich region of Sos, which results in Ras activation. The proline-rich sequences in this region of Sos that bind to Grb2 have significant homology with the class II consensus sequence. In particular, these peptides have a conserved COOH-terminal arginine,

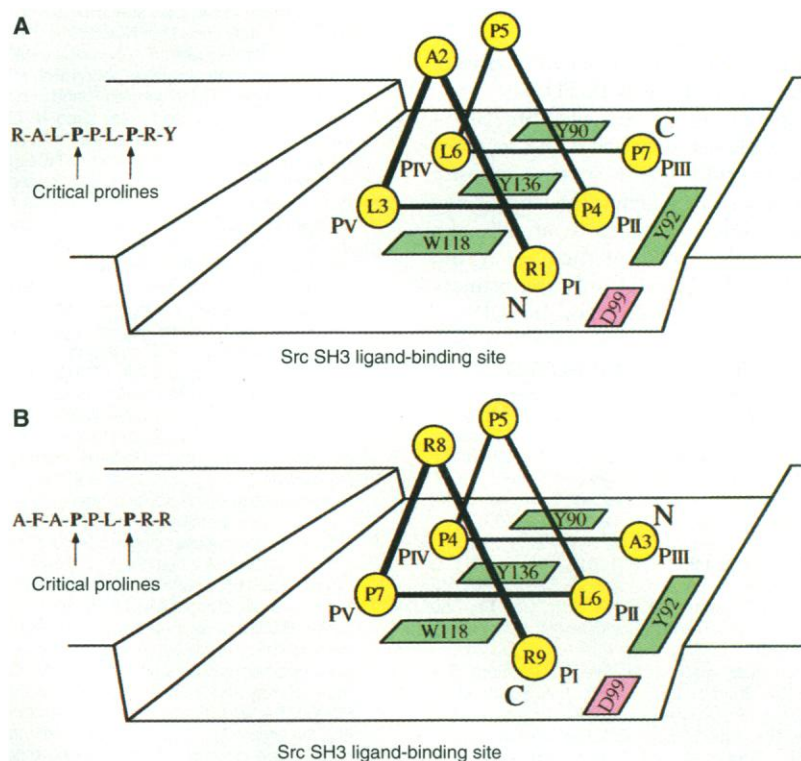


Fig. 3. Schematic representations of the RLP2 PPII helix (A) and the PLR1 PPII helix (B) at the binding site of the Src SH3 domain. Positions P₁ to P₇ are defined in the text. Ligand residues are shown in yellow, and SH3 domain residues in green and purple.

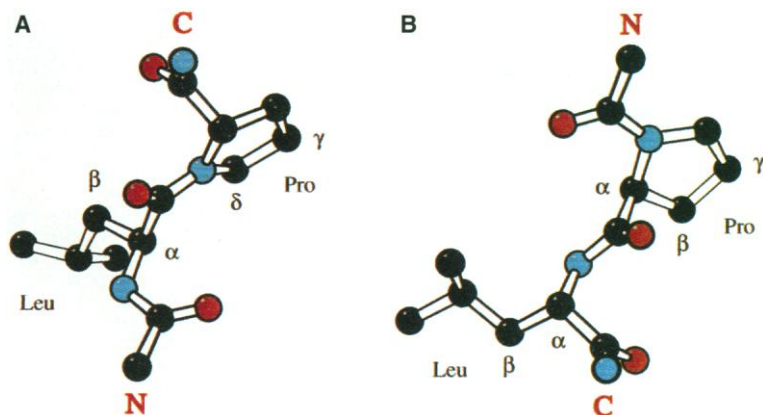


Fig. 4. Comparison of the dipeptidyl moieties XP (A) and PX (B) (X = L). Selected side chain carbons are labeled with the corresponding Greek letters. The amide backbone directionality is indicated by N and C in red. Carbon atoms are black, nitrogen atoms are blue, and oxygen atoms are red.

Table 4. Mutational analysis of Sos-derived peptides.

Peptide*	K _d (μM)†
<i>Group 1</i>	
VVPPPVP	67 ± 7
VVPAVPP	>500
VVPPAVP	159 ± 3
VVPPPVA	>500
VVPPPVA	136 ± 8
<i>Group 2</i>	
VVPPVPPRR	5.7 ± 0.2
VVPAVPPRR	65 ± 9
VVPPAVPPRR	7.6 ± 0.2
VVPPPVA	59 ± 5
VVPPPVA	9.1 ± 0.1

*Both groups of peptides had carboxamide COOH-termini. The NH₂-termini of group 1 peptides were free, whereas those of group 2 peptides were acetylated. Boldface indicates mutated residues. †K_d values for both groups of Sos peptides are means ± SD of two independent determinations with the NH₂-terminal SH3 domain of Grb2.

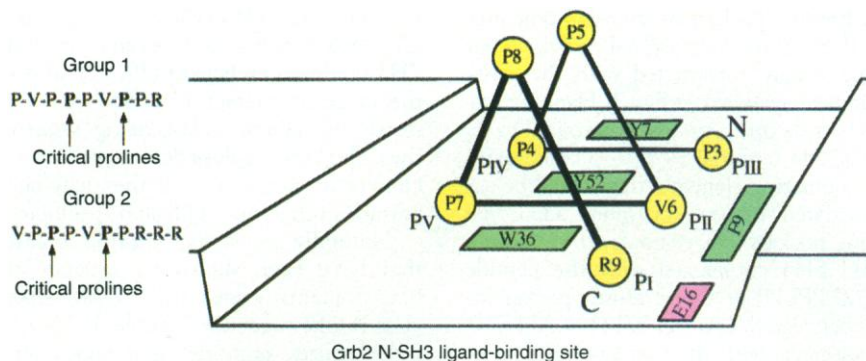


Fig. 5. Schematic representation of the Sos peptide PVPVPPR adopting a PII helix conformation at the proposed Grb2 NH₂-terminal SH3 (N-SH3) binding site.

which is essential for binding to Grb2 (24). Therefore, they should bind in the PLR orientation (5, 28).

On the basis of our general model for SH3-ligand interactions and the structure of the PLR1–Src SH3 complex, residues P4 and P7 in one of these Sos peptides, PVPPVPPR (residues 1151 to 1159 of mSos1), are predicted to be the critical contact prolines of the XPpXP motif that mediates ligand binding to the Grb2 SH3 domain, and P5 and P8 of this peptide are predicted to be the scaffolding prolines that stabilize the PII helix. The proposed PII helix of this peptide with the predicted residue positions is shown in Fig. 5. To test this model, we changed each of the four prolines individually to alanine (Table 4), and determined the affinity of the resulting peptides. In accord with the model, the P4A and P7A mutations abolished ligand binding to the NH₂-terminal SH3 domain of Grb2 (Grb2 N-SH3; residues 1 to 60 of Grb2) (29). The approximately twofold increase in K_d for the P5A and P8A mutants was anticipated because a similar effect was also observed for PLR1 and RLP1 when their scaffolding prolines were replaced by alanines. The COOH-terminal arginine R9, which is essential for Grb2 binding (24), is expected to form a salt bridge with E16 of Grb2 N-SH3, which corresponds to D99 of Src SH3 on the basis of sequence alignments.

A similar peptide with two extra COOH-terminal arginines, VPPVPPRRR (residues 1152 to 1161 of mSos1), bound to Grb2 N-SH3 with a K_d of 5.7 μ M (4). Mutational studies of this peptide (Table 4) revealed that its association with Grb2 N-SH3 is mediated by the same XPpXP motif as that of the peptide without the two extra arginines. Thus, the two groups of peptides are binding in the same frame. Sequential removal of these two arginines resulted in successive decreases in binding affinity, indicating that the two arginines also interact with the receptor. Therefore, additional residues COOH-terminal to X₁ of the class II consensus, like residues NH₂-terminal to X₁

of the class I consensus, increase the affinity of binding interactions with SH3.

The structures of the two Src SH3–ligand complexes reveal that the receptor can bind peptide ligands in two opposite orientations. More generally, they have led to a simple procedure to analyze the interactions that occur at the SH3–ligand interface on the basis of only the primary sequences of the receptor and ligand.

REFERENCES AND NOTES

- J.-Y. Kato *et al.*, *Mol. Cell. Biol.* **6**, 4155 (1986); W. M. Potts, A. B. Reynolds, T. J. Lansing, J. T. Parsons, *Oncogene Res.* **3**, 343 (1988); S. P. Nemeth, L. C. Fox, M. DeMarco, J. S. Brugge, *Mol. Cell. Biol.* **9**, 1109 (1989); C. Seidel-Dugan, B. E. Meyer, S. M. Thomas, J. S. Brugge, *ibid.* **12**, 1835 (1992).
- C. A. Koch, D. Anderson, M. F. Moran, C. Ellis, T. Pawson, *Science* **252**, 668 (1991); A. Musacchio, T. Gibson, V.-P. Lehto, M. Saraste, *FEBS Lett.* **307**, 55 (1992); T. Pawson and G. D. Gish, *Cell* **71**, 359 (1992); T. Pawson and J. Schlessinger, *Curr. Biol.* **3**, 434 (1993).
- P. Cicchetti, B. J. Mayer, G. Thiel, D. Baltimore, *Science* **257**, 803 (1992); Z. Weng, J. A. Taylor, C. E. Turner, J. S. Brugge, C. Seidel-Dugan, *J. Biol. Chem.* **268**, 14956 (1993); E. T. Barford *et al.*, *ibid.*, p. 26059; I. Gout *et al.*, *Cell* **75**, 25 (1993); X. Liu, L. E. Marengere, C. A. Koch, T. Pawson, *Mol. Cell. Biol.* **13**, 5225 (1993); S. J. Taylor and D. Shalloway, *Nature* **368**, 867 (1994); S. Fumagalli, N. F. Totty, J. J. Hsuan, S. A. Courtneidge, *ibid.*, p. 871.
- J. K. Chen, W. S. Lane, A. W. Brauer, A. Tanaka, S. L. Schreiber, *J. Am. Chem. Soc.* **115**, 12591 (1993).
- H. Yu *et al.*, *Cell* **76**, 933 (1994).
- Abbreviations for the amino acid residues are: A, Ala; C, Cys; D, Asp; E, Glu; F, Phe; G, Gly; H, His; I, Ile; K, Lys; L, Leu; M, Met; N, Asn; P, Pro; Q, Gln; R, Arg; S, Ser; T, Thr; V, Val; W, Trp; and Y, Tyr. Mutations are indicated with the single-letter code; thus, Asp⁹⁹ to Asn is represented by D99N.
- A. Musacchio, M. Saraste, M. Wilmanns, *Nature Struct. Biol.* **1**, 546 (1994).
- The c-Src SH3 domain we used contains residues 85 to 140, and the procedures for the expression and purification of the SH3 domain have been described previously (12). The residue numbering system used throughout the text is that of full-length c-Src from chicken. ¹⁵N-labeled and ¹³C-¹⁵N doubly labeled RLP2 and RLP1 were produced as described for RLP1 (5). The NMR samples contained ~3 mM of a 1:1 complex of the c-Src SH3 domain and ligand, in a D₂O or a 90% H₂O and 10% D₂O buffer containing 50 mM potassium phosphate (pH 6.0) and 150 mM KCl.
- All NMR spectra were recorded at 25°C with Bruker AMX600 and AM500 spectrometers. Most of the assignments of the complexed SH3 domain are closely similar or identical to those of the unbound state (12). The resonances belonging to the perturbed residues were assigned by two-dimensional (2D) homonuclear double quantum-filtered correlation spectroscopy (DQF-COSY) [U. Piantini, O. W. Sørensen, R. R. Ernst, *J. Am. Chem. Soc.* **104**, 6800 (1982); N. Müller, R. R. Ernst, K. Wüthrich, *ibid.* **108**, 6482 (1986)], total correlation spectroscopy (TOCSY) [A. Bax and D. G. Davis, *J. Magn. Reson.* **65**, 355 (1985)], and nuclear Overhauser effect spectroscopy (NOESY) spectra [S. Macura, Y. Huang, D. Suter, R. R. Ernst, *ibid.* **43**, 259 (1981)]. The 3D HCCH-TOCSY experiments were used to assign the spin systems of bound RLP2 and RLP1 [A. Bax, G. M. Clore, A. M. Gronenborn, *ibid.* **88**, 425 (1990)]. The amide-based assignments for RLP2 and RLP1 were performed with 2D ¹⁵N-filtered NOESY experiments performed on a 1:1 complex of ¹⁵N-labeled Src SH3 and the unlabeled ligand [A. Bax and M. Ikura, *J. Am. Chem. Soc.* **114**, 2433 (1992)].
- Interproton distances of the SH3 domain were derived from the 2D NOESY spectra with mixing times of 50 and 150 ms. The NOESY-¹H-¹³C-heteronuclear multiple-quantum coherence (HMQC) ($\tau = 100$ ms) experiments were performed with a 1:1 complex of the ¹³C, ¹⁵N-labeled ligand and the unlabeled SH3 domain, and were used to obtain intramolecular nuclear Overhauser effects (NOEs) within each ligand and intermolecular NOEs between the ligand and the protein [E. P. R. Zuiderweg and S. W. Fesik, *Biochemistry* **28**, 2387 (1989); D. Marion *et al.*, *ibid.*, p. 6150]. Most of the intermolecular NOEs are between aliphatic protons of the ligand and aromatic protons of the SH3 domain, and can be readily identified. NOE cross-peak intensities were calibrated with the 50-ms mixing time NOESY spectra based on known distances in regular secondary structural elements. NOE restraints were grouped into three ranges: 1.8 to 2.7 Å, 1.8 to 3.3 Å (1.8 to 3.5 Å for NOEs involving NH protons), and 1.8 to 5.0 Å, for strong, medium, and weak NOEs, respectively. An additional 0.5 Å was added to the upper limits for distances involving methyl groups. Hydrogen bond restraints ($1.5 \leq d_{\text{NH}\cdots\text{O}} \leq 2.3$ Å, $2.4 \leq d_{\text{NH}\cdots\text{O}} \leq 3.3$ Å) were derived from the slowly exchanging amide protons that were identified by the 2D NOESY and 2D ¹⁵N-¹H heteronuclear single-quantum coherence (HSQC) [A. Bax, R. H. Griffey, B. L. Hawkins, *J. Am. Chem. Soc.* **105**, 7188 (1983)] spectra recorded ~3 hours after dissolving the lyophilized protein in a D₂O buffer. Backbone ϕ torsional angle restraints were derived from the ³J_{NH-C α -H} coupling constants that were obtained qualitatively from the HMQC-J spectra [L. E. Kay and A. Bax, *J. Magn. Reson.* **86**, 110 (1990)]. The values for ϕ were restricted to $-120^\circ \pm 40^\circ$ for large ³J_{NH-C α -H} coupling constants and to $-55^\circ \pm 35^\circ$ for small ³J_{NH-C α -H} coupling constants. Side chain χ_1 angle restraints were based on C α -H/C β -H cross-peak magnitudes measured in a DQF-COSY spectrum and on intraresidue NOE data. In all instances, χ_1 values were restricted to a range of $\pm 60^\circ$, allowing stereospecific assignment of side chain protons based on NOEs from NH and C α -H.
- The 3D structures were calculated from the experimental restraints with the program X-PLOR 2.0, according to the reported protocol [A. T. Brünger, *X-PLOR Manual* (Yale Univ. Press, New Haven, CT, 1988); S. W. Michnick, M. K. Rosen, T. J. Wandless, M. Karplus, S. L. Schreiber, *Science* **252**, 836 (1991)]. The generated structures were refined with the simulated annealing refinement protocol described in X-PLOR 3.1 with minor modifications [A. T. Brünger, *X-PLOR Manual V. 3.1* (Yale Univ. Press, New Haven, CT, 1992)]. The refinement protocol contains a slow-cooling stage with the starting temperature at 2000 K followed by 1000 steps of conjugate gradient energy minimizations. As in our structure determination of the unbound Src SH3 domain (12), the first eight residues of the complexed protein do not have defined conformations in solution. These residues were not included in the structure calculations.
- H. Yu *et al.*, *Science* **258**, 1665 (1992).
- Y. Patterson, S. W. Englander, H. Roder, *ibid.* **249**, 755 (1990); A. R. Viguera, J. C. Martinez, V. V. Filimonov, P. L. Mateo, L. Serrano, *Biochemistry* **33**, 2142 (1994).

14. On RLP2 complexation, the indole NH proton of W118 could not be detected in the NMR spectra obtained in H₂O. This attenuation in intensity is probably not caused by rapid exchange of the NH proton, but instead may be attributed to slow conformational averaging that results in line broadening. The HSQC spectra of both complexes showed that the ¹⁵N-¹H correlations of other amide protons at the binding site also have severely attenuated intensities and broadened line widths. In the HSQC spectrum taken with the PLR1-SH3 complex, the ¹⁵N-¹H cross-peak of the indole NH of W118 appeared as a weak signal with broadened line width.
15. Structures calculated with the salt bridge restraints are consistent with the experimental data and show good geometry.
16. The D99N mutant was constructed by mutagenesis using polymerase chain reaction according to the megaprimer method [G. Sarker and S. S. Sommer, *BioTechniques* **8**, 404 (1990)]. Procedures for the expression and purification of the mutant were similar to those described for the wild-type SH3 domain (12). The D99N mutant protein was correctly folded as shown by a 2D NOESY spectrum.
17. Mutating each of the last two residues of RLP2 to alanine had only a small effect on binding affinity.
18. The significance of a PXXP motif in SH3-ligand recognition was first recognized and brought to our attention by D. Baltimore and colleagues.
19. R. Ren, B. J. Mayer, P. Cicchetti, D. Baltimore, *Science* **259**, 1157 (1993).
20. In both binding orientations, the two critical prolines of the XPPXP motif intercalate into the binding site primarily via the γ and δ methylenes of the proline rings (Fig. 4A), whereas the first and fourth prolines in the PXXPX sequence would interact with the binding site mainly via the β and γ proline methylenes (Fig. 4B). This observation provides an alternative mnemonic device to facilitate the identification of important prolines in an SH3-binding polyproline helix.
21. The affinities of these two PX peptides for D99N SH3 were further decreased, suggesting that the two peptides bind in the expected orientations.
22. SH3-binding sequences from Btk and CDC42 GAP (guanosine triphosphatase activating protein) have lysine at the X₁ site (Table 3).
23. P. Finan *et al.*, *J. Biol. Chem.* **269**, 13752 (1994).
24. M. Rozakis-Adcock, R. Fernley, J. Wade, T. Pawson, D. Bowtell, *Nature* **363**, 83 (1993).
25. R. Kapeller *et al.*, *J. Biol. Chem.* **269**, 1927 (1994); K. Seedorf *et al.*, *ibid.*, p. 16009; S. Tanaka *et al.*, *Proc. Natl. Acad. Sci. U.S.A.* **91**, 3443 (1994); H. Sumimoto *et al.*, *ibid.*, p. 5345; M. Sudol, *Oncogene* **9**, 2145 (1994); G. Cheng, Z.-S. Ye, D. Baltimore, *Proc. Natl. Acad. Sci. U.S.A.* **91**, 8152 (1994); R. Rickles *et al.*, *EMBO J.* **13**, 5598 (1994).
26. C. M. Pleiman, W. M. Hertz, J. C. Cambier, *Science* **263**, 1609 (1994); J. K. Chen and S. L. Schreiber, *Bioorg. Med. Chem. Lett.* **4**, 1755 (1994).
27. A. A. Adzhubei and M. J. E. Sternberg, *J. Mol. Biol.* **229**, 472 (1993).
28. W. A. Lim and F. M. Richards, *Nature Struct. Biol.* **1**, 221 (1994).
29. Sos has an in vitro binding preference for the NH₂-terminal Grb2 SH3 domain [K. Reif, L. Buday, J. Downward, D. A. Cantrell, *J. Biol. Chem.* **269**, 14081 (1994)]. The complementary DNA encoding the NH₂-terminal SH3 domain of Grb2 (residues 1 to 60) was amplified from a human brain stem library, and the polymerase chain reaction product was subcloned into the pGEX-2TK vector (Pharmacia). Expression of the construct in *Escherichia coli* strain BL-21 yielded a glutathione-S-transferase-SH3 fusion protein, which was purified with a glutathione-Sepharose column (Pharmacia LKB) and cleaved with thrombin (Sigma). The cleavage mixture was purified by exclusion chromatography on Sephacryl S-100 (Pharmacia).
30. B. R. Brooks *et al.*, *J. Comput. Chem.* **4**, 187 (1983).
31. A. Nicholls, K. A. Sharp, B. Honig, *Protein Struct. Funct. Genet.* **11**, 281 (1991).
32. We thank C. G. Anklin (Bruker Instruments) and D. C. Dalgarno (ARIAD Pharmaceuticals) for assisting

in the acquisition of several NMR data sets. Supported by the National Institute of General Medical Sciences (GM44993). J.K.C. is an NSF predoctoral fellow and the recipient of an American Chemical Society Division of Organic Chemistry graduate

student fellowship; J.A.S. is an NIH postdoctoral fellow; S.L.S. is an investigator with the Howard Hughes Medical Institute.

27 July 1994; accepted 5 October 1994

A Central Role of Salicylic Acid in Plant Disease Resistance

Terrence P. Delaney,* Scott Uknes,* Bernard Vernooij, Leslie Friedrich, Kris Weymann, David Negrotto, Thomas Gaffney, Manuela Gut-Rella, Helmut Kessmann, Eric Ward, John Ryals†

Transgenic tobacco and *Arabidopsis thaliana* expressing the bacterial enzyme salicylate hydroxylase cannot accumulate salicylic acid (SA). This defect not only makes the plants unable to induce systemic acquired resistance, but also leads to increased susceptibility to viral, fungal, and bacterial pathogens. The enhanced susceptibility extends even to host-pathogen combinations that would normally result in genetic resistance. Therefore, SA accumulation is essential for expression of multiple modes of plant disease resistance.

Plants have evolved complex, integrated defense mechanisms against disease that include preformed physical and chemical barriers, as well as inducible defenses such as the production of antimicrobial compounds, enhanced strengthening of cell walls, and the production of various antifungal proteins (1). Together, these systems form an effective defense against infection, with disease resulting as a rare outcome in the spectrum of plant-microbe interactions. Infectious disease can result when a pathogen is able to overcome the defense processes of a host plant by either actively suppressing or outcompeting them. The ability of a plant to respond to an infection is determined by genetic traits in both the host and pathogen. Many plant resistance (R) genes recognize pathogen molecules resulting from the expression of so-called avirulence (avr) genes (2). This interaction often triggers a signal transduction cascade leading to a rapid, host-cell collapse at the site of infection called the hypersensitive reaction (HR) (3). Plants also possess an inducible resistance mechanism called systemic acquired resistance (SAR). In experiments with transgenic tobacco plants expressing the bacterial salicylate hydroxylase (*nahG*) gene (NahG plants), we showed that SAR re-

quires the accumulation of SA for its expression (4, 5).

The inability to express SAR in NahG tobacco was also accompanied by larger tobacco mosaic virus (TMV) lesions in these plants than in wild-type (Xanthi) plants (Fig. 1). Eventually, TMV lesions expanded from the leaf to the stem on infected NahG plants. Stem dissection showed that all tissues, including the vascular tissue, had undergone necrosis, which was associated with the presence of viral RNA as determined by RNA hybridization experiments (6). Stem necrosis was observed consistently in NahG plants, but not in Xanthi plants. Interestingly, the virus moved virtually unchecked in a cell-to-cell manner, but did not gain access to the phloem and move systemically as it would have in genetically susceptible tobacco plants (7).

To determine if increased disease susceptibility was a general feature of NahG plants, we evaluated the development of disease symptoms caused by bacterial and fungal pathogens. NahG plants showed more severe disease symptoms than wild-type plants when inoculated with *Pseudomonas syringae* pv. *tabaci*, *Phytophthora parasitica*, or *Cercospora nicotianae* (Table 1). *Arabidopsis thaliana* ecotype Columbia (Col-0) plants that express the *nahG* gene (8) also showed enhanced susceptibility to pathogens. The bacterial pathogen *P. syringae* pv. *tomato* DC3000 (DC3000) is virulent on Col-0 plants and causes symptoms resembling the bacterial speck disease of tomato (9). On Col-0 plants, DC3000 caused the formation of small, chlorotic spots on inoculated leaves that were associated with an increase of four to five orders of magnitude in bacterial titer over 5 days (Fig. 2A). However,

T. P. Delaney, S. Uknes, B. Vernooij, L. Friedrich, K. Weymann, D. Negrotto, T. Gaffney, E. Ward, J. Ryals, Agricultural Biotechnology Research Unit, Ciba-Geigy Corporation, P.O. Box 12257, Research Triangle Park, NC, USA.

M. Gut-Rella, Seeds Division, Ciba-Geigy, Ltd., CH-4002 Basel, Switzerland.

H. Kessmann, Plant Protection Division, Ciba-Geigy, Ltd., CH-4002 Basel, Switzerland.

*These authors contributed equally to this study.

†To whom correspondence should be addressed.